

RESEARCH ARTICLE SUMMARY

NEUROEVOLUTION

Cell-type profiling in salamanders identifies innovations in vertebrate forebrain evolution

Jamie Woych†, Alonso Ortega Gurrola†, Astrid Deryckere†, Eliza C. B. Jaeger†, Elias Gumnit†, Gianluca Merello, Jiacheng Gu, Alberto Joven Araus, Nicholas D. Leigh, Maximina Yun, András Simon, Maria Antonietta Tosches*

INTRODUCTION: During vertebrate evolution, the first tetrapods transitioning from water to land were confronted with new environmental challenges that required adaptive innovations in the nervous system. These innovations are exemplified in the six-layered neocortex and the dorsal ventricular ridge (DVR) of present-day mammals and sauropsids (reptiles and birds), respectively. The neocortex and DVR bear extensive similarities in terms of gene expression, connectivity, and function and therefore were thought to be homologous. However, recent developmental and adult gene expression data challenge this view, suggesting that similar molecular and functional attributes may instead have arisen through convergent evolution, not a common origin. According to this alternative view, the mammalian neocortex and sauropsid DVR arose from distinct parts of the pallium: the neocortex from the expansion of a simple three-layered cortex in the dorsal pallium of amniote ancestors and the DVR from an expansion of the ventral pallium.

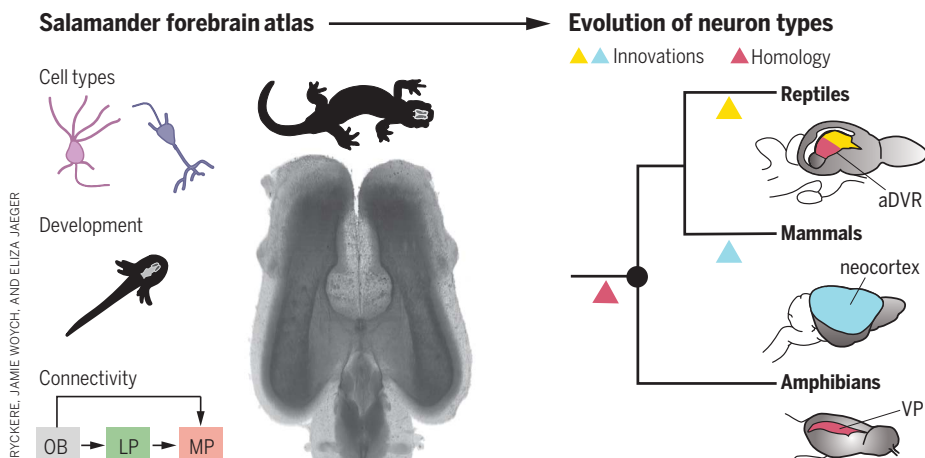
RATIONALE: If the neocortex and DVR have separate evolutionary origins, then they may

trace back to distinct pallial regions that existed in a preamniote ancestor. Amphibians diverged from other tetrapods >350 million years ago and therefore can provide crucial insights into the evolutionary history of the tetrapod brain. The amphibian telencephalon is relatively small and anatomically simple, devoid of obvious nuclei or layering, thus facilitating analysis of the entire structure. Using the salamander *Pleurodeles waltl*, a species with a true postmetamorphic adult stage, we investigated whether amphibian neuron types have transcriptomic similarity to neurons from the neocortex or DVR, probed their developmental trajectories, and characterized broad connectivity patterns.

RESULTS: Using single-cell RNA sequencing (scRNA-seq), we built a cell-type atlas of the salamander telencephalon, revealing 47 clusters of glutamatergic neurons and 67 clusters of GABAergic neurons—a greater degree of complexity and diversity than anticipated. We then mapped the expression of marker genes from select clusters using classic histology and hybridization chain reaction *in situ* hy-

bridization in cleared brains. This resulted in a three-dimensional molecular map of the salamander brain, displaying the distribution of distinct pallial regions along the mediolateral and radial axes. To characterize the developmental history of these neurons, we performed scRNA-seq on the larval *P. waltl* brain at four developmental stages. We found distinct developmental trajectories for each pallial division, indicating that distinct genetic programs specify the salamander dorsal pallium (DP) and ventral pallium (VP). To compare telencephalic neuron types across tetrapod species, we used manifold integration algorithms on scRNA-seq data from adult salamanders, reptiles (lizards and turtles), and mammals. The salamander VP shows molecular similarity to parts of the reptilian anterior DVR (aDVR), whereas the dorsomedial pallia share molecular similarities with neurons from the mammalian hippocampus, entorhinal cortex, and subiculum, but not the neocortex. This indicates that the salamander DP lacks cellular and molecular characteristics of the mammalian neocortex and is instead more similar to mammalian cortical areas intercalated between the neocortex and hippocampus. Finally, we determined whether these molecular similarities between tetrapod species are reflected in mesoscale connectivity patterns. We confirmed that salamander VP connectivity patterns resemble in part those of the reptilian aDVR and that components of the mammalian olfactory-entorhinal-hippocampal circuit exist in the salamander lateral, dorsal, and medial pallia.

CONCLUSION: These findings suggest that the aDVR in sauropsids is composed of at least two sets of neuron types with distinct evolutionary origins. While one set can be traced back to a specialized region of the anterior ventral pallium in the tetrapod ancestor, the other one is a sauropsid novelty. Additionally, we propose that pyramidal neuron types in the mammalian six-layered neocortex are evolutionary novelties that arose by changes in the gene-regulatory programs specifying ancestral types. These findings corroborate the hypothesis that the functional similarities of the DVR and neocortex are the result of convergence instead of homology. The mammalian olfactory-entorhinal-hippocampal circuit, however, may trace back to a circuit with a simpler architecture that was already present in the last common ancestor of tetrapods. ■



Reconstructing the evolution of neuron types in the vertebrate telencephalon. Amphibians are key to reconstructing the evolution of the vertebrate brain after the transition from water to land. An atlas of the salamander telencephalon, including transcriptomic profiling of cell types, developmental trajectories, and connectivity, offers new insights into the homologies and innovations of the vertebrate brain.

The list of author affiliations is available in the full article online.

*Corresponding author. Email: mt353@columbia.edu

†These authors contributed equally to this work.

Cite this article as J. Woych et al., *Science* **377**, eabp9186 (2022). DOI: 10.1126/science.abp9186

S READ THE FULL ARTICLE AT
<https://doi.org/10.1126/science.abp9186>

RESEARCH ARTICLE

NEUROEVOLUTION

Cell-type profiling in salamanders identifies innovations in vertebrate forebrain evolution

Jamie Woych^{1†}, Alonso Ortega Gurrola^{1,2†}, Astrid Deryckere^{1†}, Eliza C. B. Jaeger^{1†}, Elias Gumnit^{1†}, Gianluca Merello¹, Jiacheng Gu¹, Alberto Joven Araus³, Nicholas D. Leigh⁴, Maximina Yun^{5,6}, András Simon³, Maria Antonietta Tosches^{1*}

The evolution of advanced cognition in vertebrates is associated with two independent innovations in the forebrain: the six-layered neocortex in mammals and the dorsal ventricular ridge (DVR) in sauropsids (reptiles and birds). How these innovations arose in vertebrate ancestors remains unclear. To reconstruct forebrain evolution in tetrapods, we built a cell-type atlas of the telencephalon of the salamander *Pleurodeles waltl*. Our molecular, developmental, and connectivity data indicate that parts of the sauropsid DVR trace back to tetrapod ancestors. By contrast, the salamander dorsal pallium is devoid of cellular and molecular characteristics of the mammalian neocortex yet shares similarities with the entorhinal cortex and subiculum. Our findings chart the series of innovations that resulted in the emergence of the mammalian six-layered neocortex and the sauropsid DVR.

The transition from water to land was a pivotal moment in vertebrate history that exposed the first tetrapods to new environmental and cognitive challenges, which may have accelerated adaptive innovations in the nervous system (1). After the divergence of mammals and sauropsids (reptiles and birds) ~320 million years ago, innovations in the pallium (i.e., the dorsal telencephalon) paved the way for advanced cognition. In mammals, the neocortex, with its characteristic six layers, evolved from a simpler ancestral cortex located in the dorsal pallium (2). In sauropsids, an expansion of the ventral pallium produced a large set of nuclei called the dorsal ventricular ridge (DVR) (Fig. 1A). Although neocortex and DVR develop from different parts of the pallium, they bear extensive similarities in terms of gene expression, connectivity, and function (3–5). A model centered on brain connectivity proposes the homology of neocortex and DVR, implying that differences in neocortex and DVR development and topological positions arose secondarily (6). Developmental studies (2) and adult transcriptomics data (7, 8) challenge this view, suggesting that the DVR and neocortex have separate evolutionary origins in amniote ancestors, and there-

fore similar functions were acquired independently. However, the origin of innovations that led to the DVR and neocortex remains poorly understood at the molecular and cellular levels.

We reasoned that if neocortex and DVR have separate origins, then they may trace back to pallial regions that existed in a pre-amniote ancestor. Amphibians, which diverged from other tetrapods ~350 million years ago, have a seemingly simple telencephalic architecture that is devoid of obvious layering or large brain nuclei (Fig. 1B). Both a dorsal and a ventral pallium exist in amphibians (9), but it is unclear whether they are related in any way to neocortex and DVR. Here, we analyzed the telencephalon of *Pleurodeles waltl*, a salamander species with a true adult (postmetamorphic) stage, to determine the following: (i) Are there neuron types in the amphibian pallium with transcriptomic similarity to neocortical or DVR neurons? (ii); if so, then how do these neurons develop?; and (iii) do these neurons display patterns of connectivity similar to neocortex or DVR?

Results

A cell-type atlas of the salamander telencephalon

To build a cell-type atlas of the salamander telencephalon, we profiled entire brains and microdissected telencephali of adult *P. waltl* (see brain atlas in fig. S1 and movie S1). After single-cell RNA sequencing (scRNA-seq, 10x Genomics), reads were mapped on a new long-read de novo reference transcriptome (see the materials and methods). After quality filtering, we obtained 36,116 single-cell transcriptomes, performed Louvain clustering, and identified 11 major populations of neuronal and non-neuronal cells (Fig. 1C and fig. S2).

We annotated clusters of differentiated neurons, immature neurons, ependymoglia cells, microglia, oligodendrocytes, oligodendrocyte precursors, and other non-neuronal cells based on well-established marker genes (Fig. 1D and fig. S2C). Differentiated neurons (29,294 cells), identified by the expression of pan-neuronal markers such as *Snap25*, *Syt1*, and *Rbfox3* (i.e., NeuN), were subclustered to classify neuron types. This revealed 47 clusters of glutamatergic neurons and 67 clusters of γ -aminobutyric acid-releasing (GABAergic) neurons, which we annotated on the basis of marker genes with conserved expression across species, in situ hybridization for cluster-specific markers, and existing amphibian literature [reviewed in (10, 11)] (Fig. 1, E and F, and figs. S3 to S8).

In the salamander telencephalon, hierarchical clustering revealed four distinct groups of glutamatergic clusters (fig. S4A). One expressed *Neurod2* and *Slc17a7* (*Vglut1*) at high levels, and we named this group “cortical pallium” for its molecular similarity to the cerebral cortex of mammals and reptiles (12, 13). The remaining groups included olfactory bulb (OB) mitral and tufted cells expressing the transcription factor *Tbx21* (14), amygdala neurons expressing lower levels of *Slc17a7* and *Neurod2* and high levels of *Slc17a6* (*Vglut2*), and glutamatergic neurons in the septum expressing *Slc17a6*, *Zic2*, and *Isl1* (Fig. 1, E and F, and fig. S4A).

Telencephalic GABAergic neurons express markers of the subpallium, such as *Dlx5*, *Gad1*, and *Gad2*. We found that the amphibian subpallium includes not only neurons from lateral and medial ganglionic eminences (LGE and MGE, respectively), as previously shown (15, 16), but also from the caudal ganglionic eminence (CGE). We identified several types of striatal and septal neurons, nucleus accumbens, bed nucleus of the stria terminalis, and diagonal band neurons, as well as OB LGE-derived GABAergic interneurons (figs. S4A and S5, A to E). Telencephalic GABAergic interneurons, scattered throughout the pallium, included MGE- and CGE-derived cells (fig. S5F). These data indicate that despite its anatomical simplicity, the amphibian telencephalon harbors a greater degree of cell-type diversity than anticipated.

Spatial distribution of pallial glutamatergic neurons

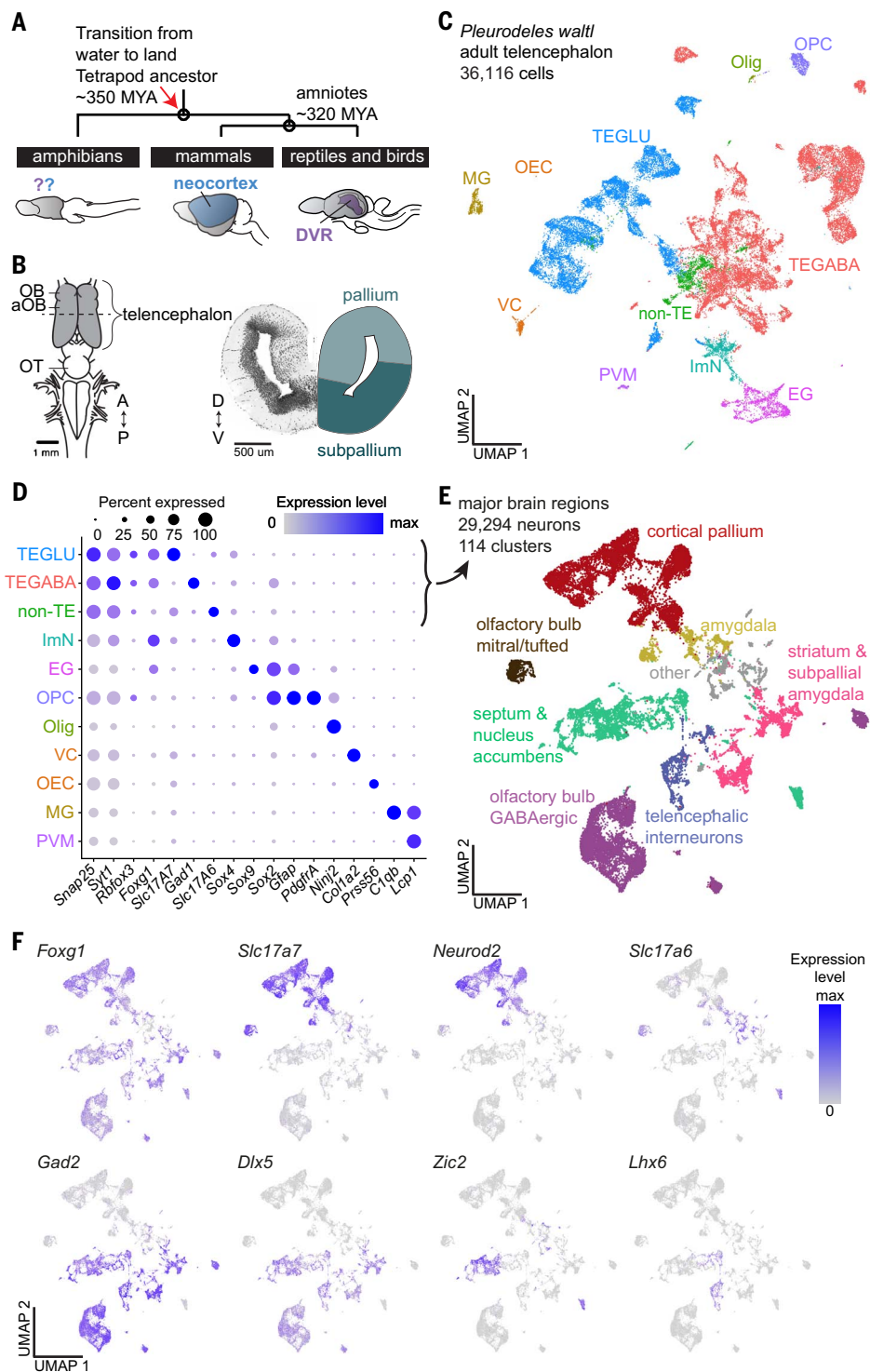
The literature indicates that the amphibian pallium is organized along the mediolateral axis in four regions called the medial, dorsal, lateral, and ventral pallium (MP, DP, LP, and VP, respectively) (9, 17), but precise boundaries and further subdivisions are a matter of dispute (18, 19) (see the supplementary text for a discussion about nomenclature). To clarify the organization of the amphibian telencephalon including the pallium, we associated clusters from scRNA-seq to their spatial

¹Department of Biological Sciences, Columbia University, New York, NY 10027, USA. ²Department of Neuroscience, Columbia University, New York, NY 10027, USA. ³Department of Cell and Molecular Biology, Karolinska Institute, SE-171 77 Stockholm, Sweden. ⁴Molecular Medicine and Gene Therapy, Wallenberg Centre for Molecular Medicine, Lund Stem Cell Center, Lund University, 221 84 Lund, Sweden. ⁵Technische Universität Dresden, CRTD/Center for Regenerative Therapies Dresden, 01307 Dresden, Germany. ⁶Max Planck Institute for Molecular Cell Biology and Genetics, 01307 Dresden, Germany.

*Corresponding author. Email: mt3353@columbia.edu

†These authors contributed equally to this work.

Fig. 1. Neuronal diversity in the *P. waltl* telencephalon. (A) Schematic highlighting the phylogenetic position of amphibians, the mammalian neocortex, and the reptilian DVR. (B) Left: schematic of the *P. waltl* brain (dorsal view). Dotted line indicates the section plane for the coronal slice on the right. (C) Uniform Manifold Approximation and Projection (UMAP) plot of 36,116 salamander single-cell transcriptomes; colors indicate cell classes. (D) Dotplot showing the expression of marker genes used to annotate the telencephalic dataset in (C). (E) UMAP plot of 29,294 single-cell transcriptomes of salamander neurons; colors indicate major brain regions. (F) UMAP plots showing expression of key markers of glutamatergic and GABAergic neurons in the neuronal dataset. A, anterior; aOB, accessory OB; D, dorsal; EG, ependymoglia; GLU, glutamatergic; ImN, immature neurons; MG, microglia; MYA, million years ago; OEC, olfactory ensheathing cells; Olig, oligodendrocytes; OPC, oligodendrocyte precursor cells; OT, optic tectum; P, posterior; PVM, perivascular macrophages; TE, telencephalic; V, ventral; VC, vascular cell.



origin and built a transcriptomics-based map of the telencephalon in *P. waltl*.

Hierarchical clustering of average cluster expression profiles indicates a clear distinction between cortical pallium and amygdala and the existence of four groups of cortical pallium clusters (Fig. 2, A and B, and fig. S4, A and B). As shown by in situ hybridization for specific marker genes (Fig. 2C), the four

groups largely correspond to MP, DP, LP, and VP. In mid-telencephalic sections, the MP, which is comparable to the hippocampus in its position and connectivity, expresses hippocampal transcription factors such as *Fezf2*, *Lhx9*, *Zbtb20*, and *Etv1* (7, 20). The DP, anatomically distinct from the MP, expresses low levels of MP markers but high levels of *Etv1*. The LP, a narrow band of densely packed neurons, ex-

presses *Lhx2*, *Satb1*, *Rorb*, and *Reln*, markers of olfactory-recipient cells in the mammalian piriform cortex (semilunar cells) (21). Most of the VP expresses the transcription factor *Sox6* and is molecularly diverse, which is consistent with its anatomical heterogeneity (9, 22). Subdivisions of VP include a *Nos1*-negative anterior VP (VPa) and a *Nos1*⁺ posterior VP (VPp) [see also (16)]. Along the anterior-posterior

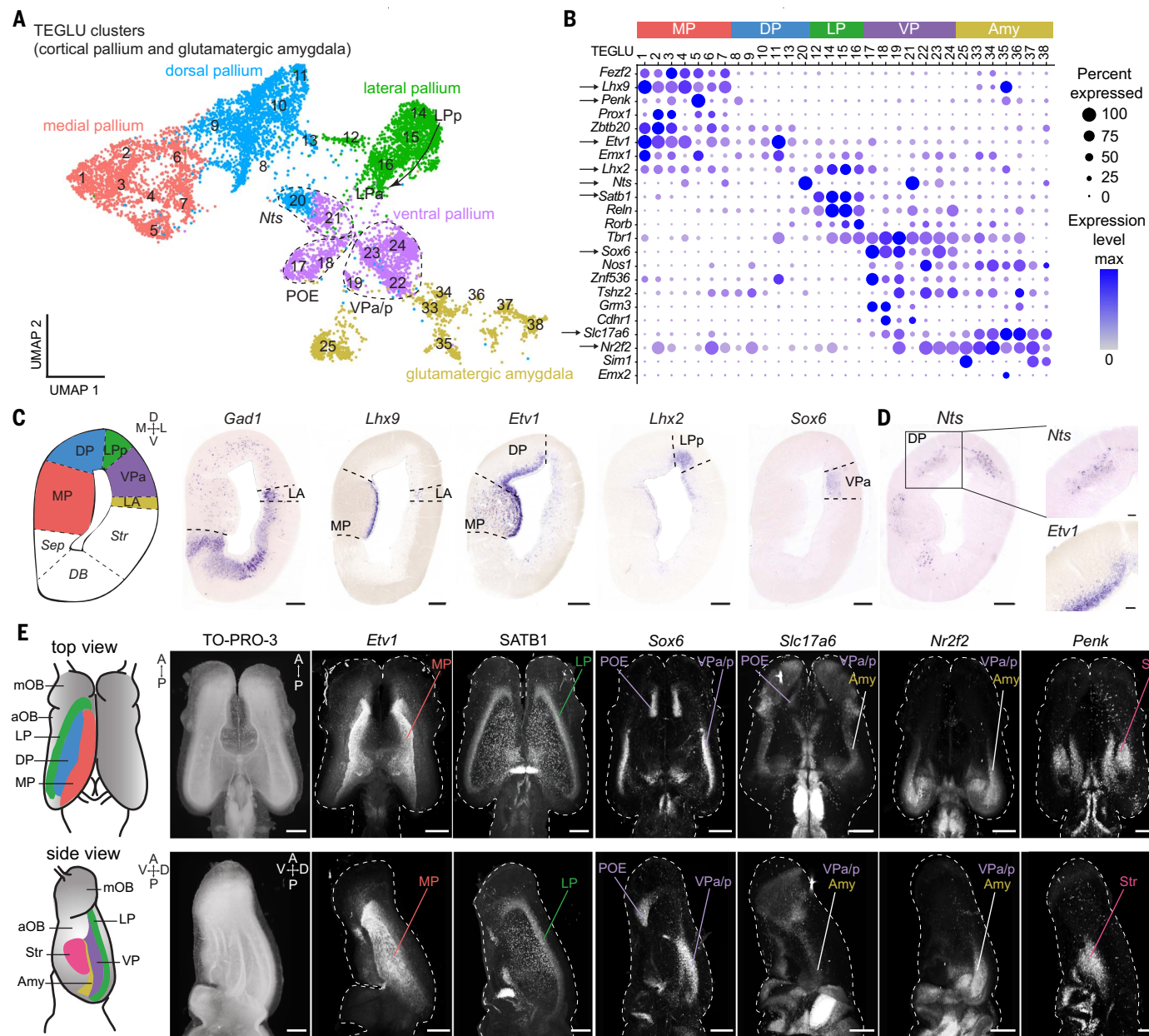


Fig. 2. Spatial mapping of pallial neurons in *P. waltli*. (A) UMAP plot of clusters from cortical pallium and amygdala, annotated by the inferred pallial region. TEGLU, telencephalic glutamatergic. (B) Dotplot showing the expression of key marker genes defining distinct pallial regions. Arrows indicate the genes shown in (C) to (E). (C) Left to right: schematic of a coronal section at the mid-telencephalic level; expression of *Gad1*, a marker of the subpallium, and of transcription factors labeling distinct pallial regions along the mediolateral axis. Scale bars: 200 μ m. (D) Expression

of *Nts* and *Etv1* in layers, boxed areas indicate magnifications on the right. Scale bars in right panels: 50 μ m. (E) Left: schematics of dorsal and lateral surfaces of the salamander telencephalon. Right: dorsal and lateral views of whole-mount immunohistochemistry or HCR stainings for telencephalic markers. Panels show maximum intensity projections of brains after clearing and volumetric light-sheet imaging. Scale bars: 500 μ m. See methods for specifics on SATB1 antibody. Amy, amygdala; for a full list of abbreviations, see fig. S1.

axis, *Slc17a6* is expressed only in the most ventral portion of the VP, suggesting the existence of further diversity along the mediolateral axis; *Slc17a6* is expressed at higher levels in the adjacent amygdala, as described in (23) (figs. S6 to S8 and movies S2 and S3). In addition to these subdivisions of VP, we found expression of *Sox6*, *Znf536*, and *Grm3* in an anterior pallial region, which is not continuous with VP but instead is nested between the OB and the

septum and corresponds to the amphibian postolfactory eminence (POE) (24, 25).

A closer look at *Nts*, a marker expressed at high levels in two clusters (Fig. 2B), revealed differential expression along the radial axis. Visualization of *Nts* expression in tandem with genes expressed in cells closer to the ventricle (e.g., *Etv1* in MP/DP) demonstrates that *Nts* demarcates a discrete, superficial layer of the pallium (Fig. 2D and fig. S6H). These results

suggest that the amphibian pallium contains at least two separate layers of distinct neuron types.

To resolve the three-dimensional (3D) organization of the pallium, we exploited the relatively small size of the salamander brain to combine whole-mount hybridization chain reaction (HCR) *in situ* hybridization, brain clearing [immunolabeling-enabled 3D imaging of solvent-cleared organs (iDISCO)], and light-sheet

imaging, creating a 3D molecular map (Fig. 2E, fig. S7, and movies S2 and S3). This revealed that the cortical pallium is organized in adjacent longitudinal stripes running the length of the telencephalic vesicle (Fig. 2E). For example, the LP extends from the most rostral tip of the pallium, where it contacts the main OB (mOB) and the POE, to the caudal tip of the telencephalon. The amygdala is localized caudally and is demarcated by the expression of *Slc17a6* and *Nr2f2* and the absence of *Sox6* (Fig. 2E, figs. S7 and S8, and movies S2 and S3). Together, these data represent a transcriptomics-based map of the amphibian pallium and support the existence of distinct regions along the mediolateral axis and distinct layers along the radial axis.

Developmental trajectories of DP and VP

How regions of the amphibian pallium compare with distinct regions of the mammalian and sauropsid pallium, including the hippocampus, olfactory cortex, and amygdala, remains debated (10, 26, 27). Current models postulate that pallial regions are homologous when they develop from homologous progenitor domains (17, 28, 29). To trace the developmental history of *P. waltl* pallial neuron types, we collected scRNA-seq data from stage 36, 41, 46, and 50 larvae (Fig. 3, A and B, and fig. S9A) [see also (30)]. After unsupervised clustering, we identified radial glia and telencephalic glutamatergic and GABAergic developing neurons (Fig. 3, C and D, and fig. S9, B and C). To assign developing neurons to their terminal fate in the adult telencephalon, we mapped adult scRNA-seq data on developmental data using the Seurat label-transfer algorithm (see the materials and methods) (31). This showed that our larval dataset included differentiating neurons from all major pallial and subpallial subdivisions (Fig. 3C and fig. S9C). We then inferred developmental trajectories for differentiation into OB mitral and tufted cells, amygdala, VP, LP, DP, and MP with Slingshot (32) (Fig. 3E). After reordering cells according to their pseudotime score, we compared gene expression along the DP and VP trajectories (fig. S9D). Transcription factors up-regulated along the dorsal trajectory included *Lhx2*, *Sox8*, and *Nfix*. Transcription factors up-regulated along the ventral trajectory included *Pbx3* and *Sox6*, which are also expressed in the developing mouse ventral pallium (33) (Fig. 3, F and G). This indicates that neurons in the DP and VP are specified by distinct gene-regulatory cascades, possibly controlled by medial *wnt* signaling and ventrolateral *wnt* antagonists (29). This analysis thus highlights clear differences in the specification of salamander DP and VP neurons, demonstrating that the distinct DP and VP clusters identified in the adult data have their own developmentally conserved transcription factor networks.

Comparison of salamander VP and reptilian anterior DVR

To identify neuron types with similar gene expression profiles in salamanders, reptiles, and mammals, we compared scRNA-seq datasets using manifold integration algorithms. We compared several data integration algorithms (fig. S11 and supplementary text) and present here the results obtained using Seurat, an algorithm based on the identification of mutual nearest neighbors across single-cell datasets (see the materials and methods) (31). For consistency and to facilitate data analysis, we limited data integration to single cells sampled from the same brain regions. We integrated our salamander dataset with data from the telencephalon of the agamid lizard *Pogona vitticeps* (34, 35) and from the pallium of the red-eared slider turtle *Trachemys scripta* [which also includes cells from the neighboring subpallium (7)]. Clustering of the Seurat integrated data yielded 65 clusters, which we refer to as integrated clusters. Results from the Seurat integration were largely recapitulated by using alternative parameters in the integration pipeline, as well as alternative integration algorithms (Harmony, SAMap, and scVI; see the supplementary text and figs. S11 and S12). Hierarchical clustering of average gene expression in integrated clusters produced a cross-species taxonomy of telencephalic neuron types (Fig. 4, A to C, and fig. S13).

This kind of analysis is built on molecular similarities of cells that result from either homology or the convergent use of the same effector genes. Here, we observed co-clustering of salamander and reptilian cells from pallial regions that are considered homologous on the basis of independent criteria such as their relative position in the pallium (2, 17). For example, we found co-clustering of salamander MP and the reptilian medial cortex and of salamander LP and the reptilian lateral cortex. The salamander pallial amygdala (23) and reptilian posterior DVR (pDVR), putative homologs of the mammalian pallial amygdala (36), also co-clustered (Fig. 4D and fig. S13). For its position in the pallium and its connectivity, the amphibian VP is a putative homolog of the reptilian ventrolateral pallium, including the anterior DVR (aDVR) (37). We found that reptilian aDVR and salamander VP neurons co-clustered in two distinct neighborhoods, segregating into a total of six clusters (3, 13, 31, 58, 17, and 30). Integrated cluster 13 included salamander cells from the VPa/VPp and turtle and lizard cells from the centromedial aDVR, an area heavily connected with the hypothalamus (Fig. 4E) (7, 37). Integrated cluster 3, in the same neighborhood, included more cells from the lizard and turtle centromedial aDVR. Turtle, lizard, and salamander cells in clusters 13 and 3 shared expression of several transcription factors, including *Tbr1*,

Nr2f2, *Nr2f1*, and *Lmo3* (Fig. 4F), supporting the hypothesis that centromedial aDVR and VP have a shared evolutionary history.

In the second neighborhood, we found cells from the rostral part of the turtle and lizard aDVR (integrated clusters 17 and 30) and from the salamander POE (integrated clusters 58 and 17). The rostral aDVR is an area receiving sensory inputs (visual, somatosensory, and auditory) relayed by the thalamus (7, 37, 38) and expresses the transcription factors *Rorb* and *Satb1* at high levels (7), as well as specific effector genes such as the glutamate receptor *Grm3* and the potassium channel *Kcnh5* (Fig. 4, E and F). The salamander POE is a pallial region primarily involved in olfaction, as suggested by its proximity to and inputs from the OB (24, 25). In *P. waltl*, we found that *Rorb* and *Satb1* are coexpressed in POE (weakly) and LP, both pallial regions with prominent olfactory inputs, but not in the VPa/VPp (Fig. 4, F and G). Furthermore, other transcription factors with specific expression in the salamander POE are not expressed in the lizard or in the turtle rostral aDVR (fig. S14), indicating that the co-clustering of neurons from these regions is driven by effector genes. The lack of transcription factor conservation between these cell types may indicate convergent use of effector genes, because only transcription factors are believed to form core regulatory complexes that track cell types as evolutionary units (39). These results indicate that the salamander ventrolateral pallium comprises neuron types with molecular similarity to reptilian lateral cortex and centromedial aDVR. Furthermore, they suggest that the sensory-recipient neurons in the rostral aDVR may have evolved by recruiting effector genes involved in sensory processing in other pallial areas.

Molecular innovations in dorsal cortex and neocortex

To extend our molecular comparisons to mammals, we computed gene expression correlations between each salamander telencephalic cluster with digitized *in situ* hybridization data from the Allen Adult Mouse Brain Atlas (40) (Fig. 5A), which confirmed the molecular similarity of salamander subpallial regions with their mouse counterparts. Results for the pallium were more ambiguous. For example, salamander LP clusters correlated with hippocampus, neocortex, piriform cortex, and lateral amygdala; pallial amygdala clusters correlated with the entire mouse pallial amygdala and piriform cortex; and VP clusters correlated with mouse piriform cortex and lateral amygdala (Fig. 5A). This is consistent with the observation that VP expresses transcription factors with specific or enriched expression in the mouse piriform cortex, such as *Znf536* and *Tshz2* (Fig. 2B and fig. S8) (40, 41). Using

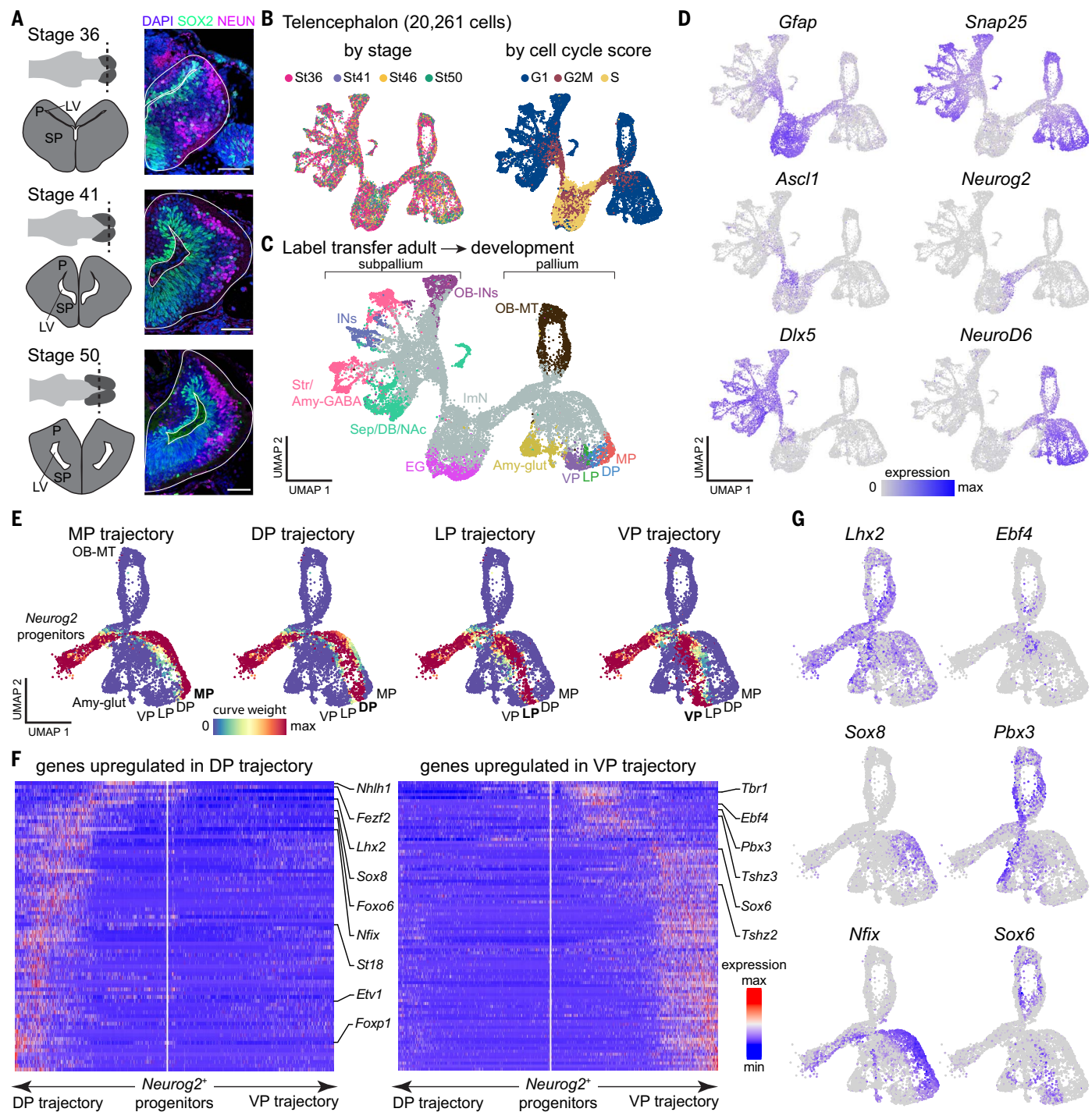


Fig. 3. Developmental trajectories in the *P. waltli* telencephalon. (A) Overview of telencephalic development in *P. waltli*. Right: coronal sections through the telencephalon showing SOX2⁺ radial glia and interneurons and NEUN⁺ differentiated neurons. Scale bars, 100 μ m. (B) UMAP plots of 20,261 telencephalic cells colored by developmental stage (left) and cell cycle score (right). (C) UMAP plot of the developing telencephalon, colored according to cell classes after label transfer from the adult dataset. (D) UMAP plots colored by the expression of *Gfap* (radial glia), *Snap25* (differentiated neurons), *Ascl1* and *Neurog2* (committed subpallial and pallial progenitors), and *Dlx5* and *NeuroD6* (post-mitotic subpallial and pallial neurons). (E) UMAP plots showing the assignment of cells to each of the trajectories on the basis of curve weights, which

represent the likelihood that a cell belongs to a given principal curve calculated by Slingshot. (F) Heatmaps of genes differentially expressed along the trajectories of the DP and VP, with transcription factors highlighted on the side. White line in the middle of each panel indicates the position of the *Neurog2*⁺ progenitors and arrows to the left and right represent the two trajectories. Gene expression levels for each gene are scaled by root mean square ranging from -2 to 6. (G) UMAP plots showing pallial single cells color-coded by expression of transcription factors up-regulated in the dorsal (left) or ventral (right) trajectory. EG, ependymoglia; ImN, immature neuron; LV, lateral ventricle; OB-MT, OB mitral and tufted cell; P, pallium; SP, subpallium; for a full list of abbreviations, see figs. S1 and S3.

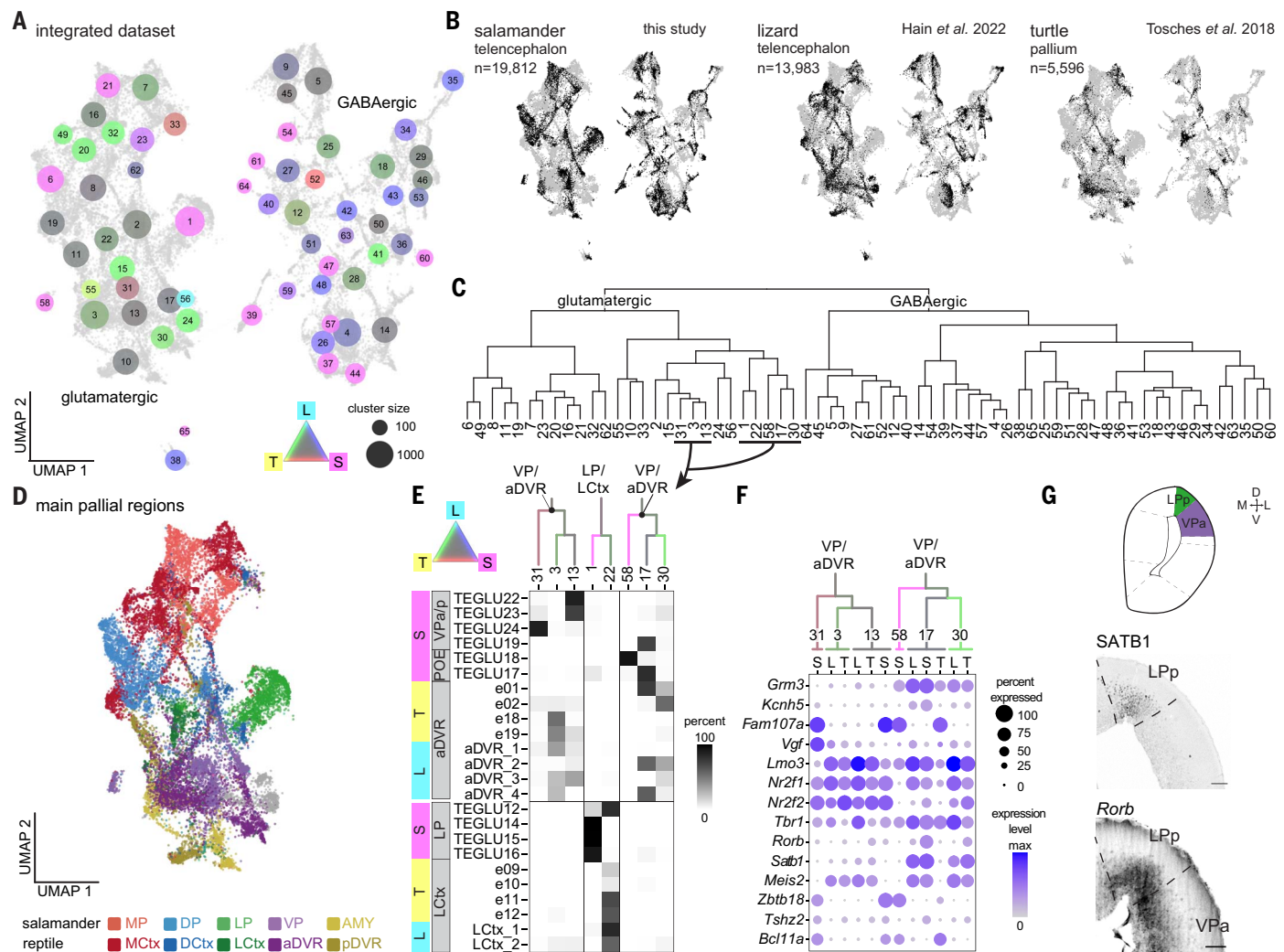


Fig. 4. Salamander and reptile telencephalon cross-species comparison.

(A) UMAP plot after integration of scRNA-seq data from the salamander and lizard telencephalon and from the turtle pallium. Dot colors indicate species mixture in each integrated cluster (gray represents an equal proportion of cells from each species). Dot size indicates the number of cells in each cluster. (B) UMAP plots of the integrated dataset showing cells from each species highlighted in black. (C) Hierarchical clustering of average expression profiles of the integrated clusters shown in (A). (D) UMAP plot of the glutamatergic clusters from the integrated dataset colored by pallial region. (E) Top: ventrolateral portion of the dendrogram in (C), with branches colored by species mixture. Bottom: percentage of cells from the original species-specific clusters (rows) in the integrated clusters (columns). (F) Dotplot showing the expression of molecular markers in aDVR or VP in the integrated clusters, with cells from each integrated cluster split by species: L, lizard; S, salamander; and T, turtle. (G) Top: schematic of a coronal section at the mid-telencephalic level in the *P. walti* brain. Bottom: presence of SATB1 and expression of *Rorb* in the salamander LP and VP. Scale bars, 100 μ m.

an alternative approach in which we mapped scRNA-seq data from the mouse telencephalon (42, 43) on our salamander single-cell dataset (see the materials and methods), we also found correspondence between the subpallial and hippocampal regions. However, using this method, mouse cortical pyramidal types could not be mapped to single salamander clusters, suggesting a high degree of transcriptional divergence (fig. S15).

We reasoned that the integration of scRNA-seq data was better suited for the identification of high-level similarities among salamander, reptilian, and mouse neuron types than mapping approaches. However, complete scRNA-seq data from the entire telencephalon of a

mammal are not yet available. In light of our results on development, we decided to focus on the derivatives of the dorsomedial pallium, which in mammals ranges from the hippocampus medially to the insular and entorhinal cortices laterally; complete mouse data are available for all of these cortical areas (43) (Fig. 5B). Telencephalic interneurons (44) were also included in this analysis. Salamander GABAergic interneurons co-clustered with amniote MGE-derived (Pvalb and Sst) and CGE-derived (Lamp5, Sncg, and Vip) interneuron classes (Fig. 5C and fig. S15B), indicating that these interneuron classes trace back to tetrapod ancestors. At deeper levels of interneuron classification, we found interneuron

types conserved in tetrapods, such as long-range projecting Sst Chodl neurons (cluster 13), and mammalian-specific types, such as Pvalb Vipr2 Chandelier cells (cluster 50) (Fig. 5C). Lamp5 interneurons included a nonmammalian subclass (cluster 34), a conserved subclass (cluster 17, Lamp5 Ndnf neurogliaform cells in mouse), and a mouse-specific subclass (cluster 49, Lamp5 Lhx6 cells) (45). The transcription factors that differentiate between mammalian Lamp5 Ndnf and Lamp5 Lhx6 interneurons are coexpressed in nonmammalian Lamp5 cells (cluster 34), suggesting that amniote or mammalian-specific Lamp5 types evolved by diversification of ancestral Lamp5 interneurons (Fig. 5D).

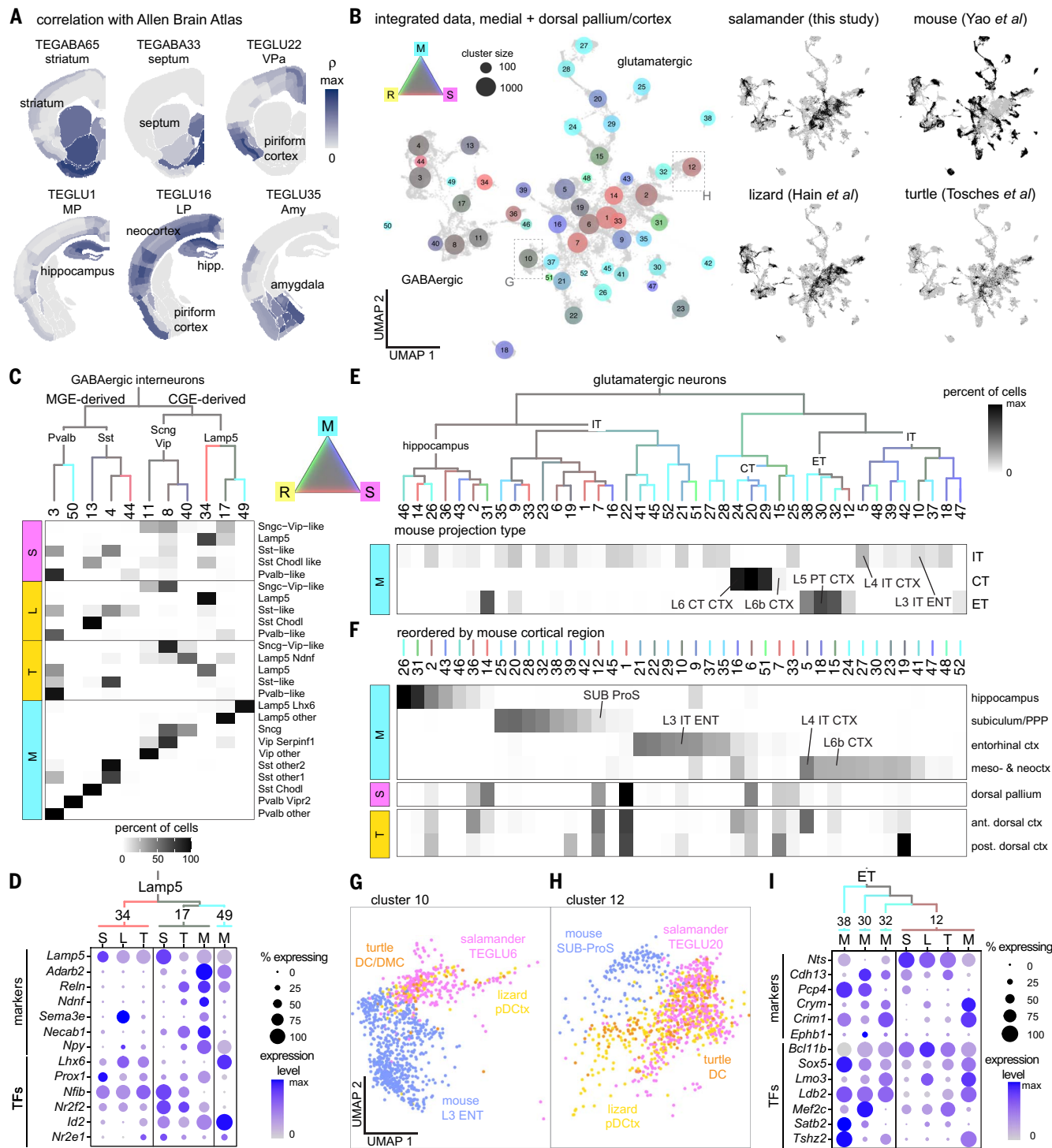


Fig. 5. Salamander, reptile, and mouse cross-species comparison. (A) Correlations of the transcriptome of selected *P. waltl* clusters with *in situ* hybridization data from the Allen Adult Mouse Brain Atlas. Correlation max is 0.3 for TEGABA33 and 0.2 for all others. (B) Integration of scRNA-seq data from the salamander MP and DP, the turtle and lizard (“reptile”) medial and dorsal cortex, and the mouse hippocampus and cortex. Left: UMAP of the integrated data with dots colored by species mixture; dot size indicates cluster size. Right: UMAP plots of the integrated dataset showing cells from each species highlighted in black. (C) Top: hierarchical clustering of average expression profiles of integrated GABAergic clusters; branches are colored by species mixture (gray represents an equal proportion of cells from each species).

Bottom: percentage of cells from the original species-specific clusters (rows) in the integrated clusters (columns). **(D)** Dotplot showing the expression of differentiation markers and of transcription factors (TFs) in Lamp5 interneurons (integrated clusters 34, 17, and 49). Cells from each integrated cluster are split by species: L, lizard; M, mouse; S, salamander; and T, turtle. **(E)** Top: Hierarchical clustering of the average expression profiles of integrated glutamatergic clusters; branches are colored by species mixture. Bottom: percentage of mouse cells in each integrated cluster (columns); mouse cells are grouped by projection identity (rows). Integrated clusters including selected mouse neuron types are highlighted. ENT, entorhinal cortex; CT, corticothalamic; IT, intratelencephalic; PT, pyramidal tract; ProS, prosubiculum; PPP, pre-,

para-, and postsubiculum; SUB, subiculum. (F) Top: percentage of mouse cells in each integrated cluster (columns); mouse cells are grouped by cortical area (rows) and columns are reordered by cortical area. Bottom: percentage of salamander DP cells and turtle dorsal cortex cells (rows) in each integrated

cluster (columns). (G and H) Magnification of part of the UMAP in (B) showing cells in cluster 10 (G) or cluster 12 (H) colored by species. (I) Dotplot showing the expression of differentiation markers and transcription factors in integrated clusters 12, 38, 30, and 32 split by species.

In the cross-species taxonomy of glutamatergic neurons, major splits corresponded to neurons with distinct projection identities in mouse: intratelencephalic neurons, extratelencephalic neurons (including L5 pyramidal tract neurons), and corticothalamic neurons (Fig. 5E and fig. S16). Several integrated clusters included neurons from mouse only, indicating a greater diversity of mouse pyramidal types. These results were largely recapitulated by integration analyses with different algorithms (fig. S17). Among the mouse-specific clusters, we identified neocortical corticothalamic and L5 pyramidal tract neurons, indicating that these neuron types have unique gene expression profiles and suggesting that they are mammalian innovations (46). Consistent with this, the transcription factor combinatorial codes that specify these types are not found in either the turtle dorsal cortex (7) or the *P. waltl* DP (fig. S16B). In Fig. 5F, we plot the same integrated clusters reordered by mouse cortical region and the proportions of salamander DP and turtle dorsal cortex neurons within these clusters. Most salamander MP and DP neurons co-clustered with mammalian neurons from the hippocampus, entorhinal cortex, and subiculum (Fig. 5, F to H, and fig. S16A). The same pattern was observed for neuron types from the reptilian cortex, but with one exception: Reptiles also have neurons that co-cluster with the neocortical thalamorecipient L4 intratelencephalic neurons (Fig. 5F). The analysis of transcription factor expression points to key differences that may underlie the diversity of pyramidal neurons in tetrapods. Some of the transcription factors instructing neuronal identity in the reptilian dorsal cortex and mammalian neocortex, such as *Satb2* and *Rorb* (47, 48), are not expressed at all in the salamander DP (Fig. 2B and fig. S16B). In other cases, there are differences in transcription factor combinatorial codes. For example, we find that mouse L5 pyramidal tract neurons (cluster 30) are grouped together with L5 neurons from the pre-, para-, and postsubiculum (cluster 38) and with other neurons from the prosubiculum and subiculum (clusters 32 and 12). Cluster 12 also includes neuron types from the salamander DP and the reptilian dorsal cortex. All of these neurons share expression of the transcription factors *Bcl11b* and *Sox5* but differ for the expression of others (Fig. 5I), supporting the concept that neuronal diversity evolves through changes of transcription factor regulatory programs. This analysis indicates that the salamander DP lacks the cellular and molecular

characteristics of the mammalian neocortex, and that DP neuron types are molecularly more similar to pyramidal neurons in the mammalian cortical areas intercalated between neocortex and hippocampus (13).

Similarities and innovations in vertebrate telencephalic connectivity

The results of our comparative analysis prompted us to investigate whether neuron types with similar transcriptomes have similar connectivity across species. Expanding on previous findings in salamanders [reviewed in (26)], we conducted retrograde tracing experiments in adult *P. waltl*. We confirmed that both anterior and posterior VP regions project to the putative ventromedial hypothalamus homolog (49) (fig. S18A). The anterior VP receives afferents from mOB, LP, and DP (Fig. 6A and fig. S19), suggesting a function in olfactory processing. Consistent with previous findings (22), VPa also sparsely receives projections from the central thalamus (Fig. 6A). The central thalamus expresses *Slc17a6* and *Calb2* and relays multimodal inputs to the telencephalon. Therefore, it is considered the amphibian homolog of amniote first-order sensory nuclei (50). In reptiles, the aDVR receives inputs from the dorsal cortex, but not from olfactory areas, and is organized in subregions innervated by thalamic visual, auditory, and somatosensory nuclei (4, 37, 51, 52). Although sensory inputs are processed separately by modality in the aDVR, there is no indication that this is the case in the salamander VP. Projections to the aDVR also include the striatum, the pDVR, and the ventromedial hypothalamus (4, 37, 53). The molecular and connectivity data suggest that reptilian aDVR neurons might have evolved from olfactory-recipient VP neurons that lost their connections to the olfactory system and became specialized in the processing of sensory inputs relayed by the thalamus (Fig. 6D and fig. S19B).

We also compared patterns of pallial connectivity in *P. waltl* with mammalian olfactory-entorhinal-hippocampal circuits. In mammals, the primary input to the hippocampal formation is the entorhinal cortex, which includes a lateral region strongly connected to olfactory areas and a medial region that processes spatial and contextual information (54). The subiculum is the primary output region of the hippocampus. Motivated by our molecular data (Fig. 5), we investigated whether the connections between salamander MP and DP are broadly analogous to the connections of mammalian hippocampus, entorhinal cortex, and

subiculum, as suggested by previous literature (9, 22, 26). Retrograde tracer injections confirmed that MP and DP are reciprocally connected (Fig. 6B and fig. S19, A and E). MP and DP also receive direct projections from the *Satb1*⁺/*Reln*⁺ LP region, an area that receives strong mOB inputs; the lateral olfactory tract runs along this region (24) (Fig. 6B and figs. S18C and S19E). Thus, LP neurons are similar to mammalian semilunar cells in the piriform cortex and fan cells in the entorhinal cortex (layer 2), both for their molecular profile [*Satb1*, *Reln*, *Lhx2*, and *Tbr1*; Fig. 2 and (21)] and their connectivity (direct inputs from the mOB and projections to the hippocampus). These findings suggest that components of mammalian olfactory-entorhinal-hippocampal circuits may trace back to tetrapod ancestors (Fig. 6D and fig. S19C).

Discussion

Our molecular data show that despite its anatomical simplicity, the salamander telencephalon harbors a complex repertoire of neuron types. The combined analysis of their molecular identity, development, and connectivity clarifies the evolution of two innovations in amniotes: the sauropsid aDVR and the mammalian neocortex.

The comparison of the reptilian aDVR and the salamander VP reveals similar and species-specific neuron types. The molecular similarities of salamander VPa/VPP neurons and neurons in the centromedial aDVR, together with the origin of these cells from a ventral pallium progenitor domain (distinct from the dorsal pallium) and the partial similarities of their connectivity (e.g., connections with the hypothalamus), suggest that the amphibian VPa/VPP and parts of the reptilian aDVR descend from a common set of neurons in tetrapod ancestors. We also identified reptilian-specific aDVR neurons that do not co-cluster with salamander VP neurons. These rostral aDVR neurons express a unique set of transcription factors (*Rorb* and *Satb1*) and receive thalamic inputs segregated by sensory modality (visual, somatosensory, and auditory, but not olfactory) (38). In light of this, we propose that neuron types in the aDVR that are specialized in processing sensory inputs relayed by the thalamus are an evolutionary innovation in the sauropsid lineage.

The homologs of these ventral pallium neurons in mammals remain ambiguous. Connectivity data point to similarities of the salamander VPa, aDVR, and the mammalian lateral amygdala, a region that receives sensory inputs relayed by the thalamus (37) and expresses some

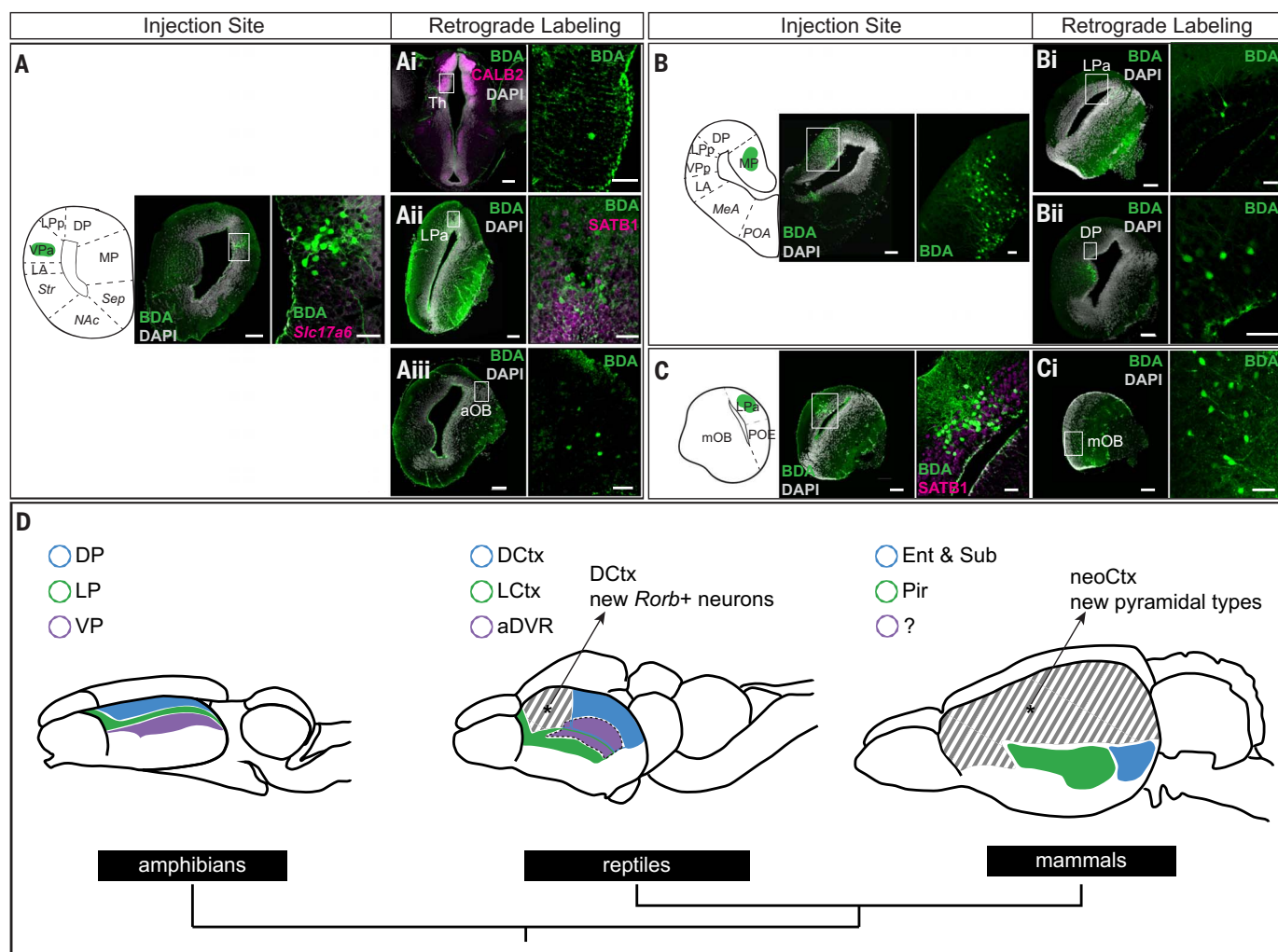


Fig. 6. Connectivity of the *P. walti* pallium. (A to C) Left: injection sites of the retrograde tracer biotinylated dextran amine (BDA). Scale bars, 200 µm. BDA (3 kDa) was injected into the VPa ($n = 4$) (A), MP ($n = 2$) (B), and LPa ($n = 2$) (C). Right: magnification of injection site with immunostaining or HCR in situ hybridization of relevant molecular markers. Scale bars, 50 µm. (Ai, Aii, Aiii, Bi, Bii, and Ci) Left: representative coronal sections in which retrogradely labeled cells were identified with immunostaining or HCR in situ hybridization of relevant molecular markers when applicable. Right: magnification of retrogradely

labeled cells with immunostaining of relevant markers when applicable. (D) Top: schematic representation of amphibian, reptile, and mammalian brains. Colors indicate molecular and connectivity similarities of neuron types across species. Cross-hatching denotes areas with cell-type innovations. MP/medial cortex, hippocampus, and mammalian subiculum are not shown in the drawing. Bottom: phylogenetic tree. DCtx, dorsal cortex; Ent, entorhinal cortex; LCtx, lateral cortex; Pir, piriform cortex; Sub, subiculum; for a full list of abbreviations, see fig. S1.

marker genes found in VPa and aDVR, such as *Rorb* (7, 26, 55). However, molecular data also indicate similarities of the salamander VPa, bird HVC [part of aDVR (8)], and mammalian piriform cortex (21) (Fig. 5A). A kinship of VPa and aDVR with parts of the mammalian piriform cortex is not surprising given that the aDVR and the sauropsid olfactory cortex develop sequentially from the same embryonic progenitors (56). Further molecular and developmental studies on the mammalian piriform cortex and pallial amygdala, the cellular diversity of which remains poorly explored, are needed to clarify their evolutionary relationships with aDVR and VPa.

Our data shed light on the nature of the amphibian DP. This region is molecularly dis-

tinct from the MP but does not express many of the markers that define the reptilian dorsal cortex, the area typically compared to the mammalian neocortex for its position, molecular makeup, and connectivity. Our cross-species analysis shows that salamander DP and several reptilian dorsal cortex neurons co-cluster with neurons of the mammalian subiculum and entorhinal cortex. The input-output connectivity of the salamander DP suggests that these molecular similarities may correspond in part to conserved circuit motifs. The *Reln*-expressing neurons in the LP occupy a peculiar position in this circuit, analogous to *Reln* neurons in the reptilian olfactory cortex and mammalian piriform (semilunar cells) and entorhinal cortex (fan cells) (21, 57). We suggest

that mammalian piriform and entorhinal *Reln*-expressing cells are serial homologs [as sister cell types (58)], with the implication that neuron types in layer 2 and in deeper layers of entorhinal cortex may have two distinct evolutionary origins from the lateral and the dorsal pallium of a tetrapod ancestor, respectively (20, 59). This scenario can be tested with molecular data from the mammalian piriform cortex.

In sum, our findings chart the series of innovations that resulted in the emergence of a six-layered neocortex in mammals (Figs. 5 and 6D). We propose that neocortical L4 *Rorb*-expressing neurons receiving sensory inputs from the thalamus evolved first, either in amniote ancestors [if salamanders retained the tetrapod ancestral state (27, 60)] or in earlier

vertebrate ancestors [with secondary loss in salamanders or amphibians (61)]. Neocortical corticothalamic neurons (L6) and pyramidal tract neurons (L5B) emerged later, in mammalian ancestors (46). Expansion of the neocortex led to functional innovations, such as the transition from distributed to columnar information processing (62) and the direct top-down control of locomotion (46). How these molecular and cellular novelties supported such functional innovations within sensory-associative pallial regions remains to be explored.

Methods summary

Animals

Adult *P. waltl* salamanders were obtained from breeding colonies established at Columbia University and Karolinska Institute. All experiments were conducted in accordance with the National Institutes of Health (NIH) guidelines and Columbia University institutional animal care and use committee policies governing animal use and welfare.

scRNA-seq library preparation

Telencephali were dissociated from either adult or larval salamanders and prepared for scRNA-seq using 10X Genomics Chromium Next GEM Single Cell 3' Kit v3.1. Sequenced libraries were aligned to a *P. waltl* reference transcriptome (see the supplementary materials and methods for details).

Analysis of scRNA-seq data

After quality filtering, scRNA-seq datasets were clustered and analyzed using the R package Seurat. For the adult data, high-level neuronal and non-neuronal clusters were first identified. Then, the neuronal dataset was subsetted and re-clustered to identify subclusters. Final clusters were annotated on the basis of the expression of established marker genes.

The quality-filtered developmental data were merged into a single object, and non-neuronal cells were filtered out. These data were regressed for cell cycle score, in addition to RNA count, stage, and percentage of mitochondrial genes, before cluster annotation.

Cross-species comparisons of transcriptomics data

Using Seurat's integration pipeline, we generated two integrated datasets using scRNA-seq data from the turtle pallium (7), the lizard telencephalon (35), and the mouse cortex and hippocampal formation (43). Average cluster expression profiles were computed, distances were computed as $1 - \text{cor}(x)$ (Spearman correlation), and this distance matrix was used for hierarchical clustering with the Ward.D2 method to generate dendograms (Figs. 4 and 5). Dendograms were color-coded according to the proportion of each species' cells in the integrated cluster. Additional annotation of the

integrated clusters was performed by analyzing the identities of each species' cells that were contained in each integrated cluster (see the supplementary materials and methods for details).

Trajectory inference

Trajectories were calculated using Slingshot to end points defined by label transfer against adult neurons. Genes that define the dorsal and ventral trajectories were calculated using Seurat's FindMarkers function. Pseudotime values provided by Slingshot were used to generate heatmaps of differentially expressed genes along each trajectory.

Immunohistochemistry and colorimetric and fluorescence in situ hybridization

Immunohistochemistry and colorimetric in situ hybridization were performed on floating sections of the adult brain or frozen sections of larval brains following standard protocols. The hybridization chain reaction protocol from Molecular Instruments was implemented and combined with iDISCO tissue clearing and light sheet imaging to generate 2D and 3D representations of gene expression (see the supplementary materials and methods for details).

Axonal tracing

Dextran amine tracer injections were performed ex vivo and brains were incubated for 24 to 48 hours. The tracer injection site and retrogradely or anterogradely labeled cells were visualized on floating sections and annotated using co-staining for known molecular markers and anatomical landmarks (see the supplementary materials and methods for details).

REFERENCES AND NOTES

- M. A. MacIver, B. L. Finlay, The neuroecology of the water-to-land transition and the evolution of the vertebrate brain. *Philos. Trans. R. Soc. Lond. B Biol. Sci.* **377**, 20200523 (2022). doi: [10.1098/rstb.2020.0523](https://doi.org/10.1098/rstb.2020.0523); pmid: [34957852](https://pubmed.ncbi.nlm.nih.gov/34957852/)
- G. F. Striedter, The telencephalon of tetrapods in evolution. *Brain Behav. Evol.* **49**, 179–213 (1997). doi: [10.1159/000112991](https://doi.org/10.1159/000112991); pmid: [9096908](https://pubmed.ncbi.nlm.nih.gov/9096908/)
- A. B. Butler, Z. Molnár, Development and evolution of the collicopallium in amniotes: A new hypothesis of field homology. *Brain Res. Bull.* **57**, 475–479 (2002). doi: [10.1016/S0361-9230\(01\)00679-7](https://doi.org/10.1016/S0361-9230(01)00679-7); pmid: [12192301](https://pubmed.ncbi.nlm.nih.gov/12192301/)
- A. B. Butler, A. Reiner, H. J. Karten, Evolution of the amniote pallium and the origins of mammalian neocortex. *Ann. N. Y. Acad. Sci.* **1225**, 14–27 (2011). doi: [10.1111/j.1749-6632.2011.06006.x](https://doi.org/10.1111/j.1749-6632.2011.06006.x); pmid: [21534989](https://pubmed.ncbi.nlm.nih.gov/21534989/)
- E. D. Jarvis, "The evolution of vocal learning systems in birds and humans," in *Evolution of Nervous Systems*, J. H. Kaas, Ed. (Elsevier, 2007), pp. 213–227.
- H. J. Karten, Neocortical evolution: Neuronal circuits arise independently of lamination. *Curr. Biol.* **23**, R12–R15 (2013). doi: [10.1016/j.cub.2012.11.013](https://doi.org/10.1016/j.cub.2012.11.013); pmid: [23305661](https://pubmed.ncbi.nlm.nih.gov/23305661/)
- M. A. Tosches et al., Evolution of pallium, hippocampus, and cortical cell types revealed by single-cell transcriptomics in reptiles. *Science* **360**, 881–888 (2018). doi: [10.1126/science.aar4237](https://doi.org/10.1126/science.aar4237); pmid: [29724907](https://pubmed.ncbi.nlm.nih.gov/29724907/)
- B. M. Colquitt, D. P. Merullo, G. Konopka, T. F. Roberts, M. S. Brainard, Cellular transcriptomics reveals evolutionary identities of songbird vocal circuits. *Science* **371**, eabd9704 (2021). doi: [10.1126/science.abd9704](https://doi.org/10.1126/science.abd9704); pmid: [33574185](https://pubmed.ncbi.nlm.nih.gov/33574185/)
- R. G. Northcutt, E. Kicliter, "Organization of the amphibian telencephalon," in *Comparative Neurology of the Telencephalon*, S. O. E. Ebbesson, Ed. (Springer, 1980), pp. 203–255.
- A. González, J. M. López, R. Morona, N. Moreno, "The organization of the central nervous system of amphibians," in *Evolutionary Neuroscience*, J. H. Kaas, Ed. (Elsevier, 2020), pp. 125–157.
- W. J. Smeets, O. Marín, A. González, Evolution of the basal ganglia: New perspectives through a comparative approach. *J. Anat.* **196**, 501–517 (2000). doi: [10.1046/j.1469-7580.2000.19640501.x](https://doi.org/10.1046/j.1469-7580.2000.19640501.x); pmid: [10923983](https://pubmed.ncbi.nlm.nih.gov/10923983/)
- I. Bormuth et al., Neuronal basic helix-loop-helix proteins Neurod2/6 regulate cortical commissure formation before midline interactions. *J. Neurosci.* **33**, 641–651 (2013). doi: [10.1523/JNEUROSCI.0899-12.2013](https://doi.org/10.1523/JNEUROSCI.0899-12.2013); pmid: [23303943](https://pubmed.ncbi.nlm.nih.gov/23303943/)
- L. Puelles, A. Alonso, E. García-Calero, M. Martínez-de-la-Torre, Concentric ring topology of mammalian cortical sectors and relevance for patterning studies. *J. Comp. Neurol.* **527**, 1731–1752 (2019). doi: [10.1002/cne.24650](https://doi.org/10.1002/cne.24650); pmid: [30737959](https://pubmed.ncbi.nlm.nih.gov/30737959/)
- A. Faedo et al., Developmental expression of the T-box transcription factor T-bet/Tbx21 during mouse embryogenesis. *Mech. Dev.* **116**, 157–160 (2002). doi: [10.1016/S0925-4773\(02\)00114-4](https://doi.org/10.1016/S0925-4773(02)00114-4); pmid: [12128215](https://pubmed.ncbi.nlm.nih.gov/12128215/)
- N. Moreno, A. González, S. Rétaux, Evidences for tangential migrations in *Xenopus* telencephalon: Developmental patterns and cell tracking experiments. *Dev. Neurobiol.* **68**, 504–520 (2008). doi: [10.1002/dneu.20603](https://doi.org/10.1002/dneu.20603); pmid: [18214835](https://pubmed.ncbi.nlm.nih.gov/18214835/)
- N. Moreno, A. González, Regionalization of the telencephalon in urodele amphibians and its bearing on the identification of the amygdaloid complex. *Front. Neuroanat.* **1**, 1 (2007). doi: [10.3389/neuro.05.001.2007](https://doi.org/10.3389/neuro.05.001.2007); pmid: [18958195](https://pubmed.ncbi.nlm.nih.gov/18958195/)
- A. Brox, L. Puelles, B. Ferreiro, L. Medina, Expression of the genes *Enx1*, *Tbr1*, and *Eomes* (*Tbr2*) in the telencephalon of *Xenopus laevis* confirms the existence of a ventral pallial division in all tetrapods. *J. Comp. Neurol.* **474**, 562–577 (2004). doi: [10.1002/cne.20152](https://doi.org/10.1002/cne.20152); pmid: [15174073](https://pubmed.ncbi.nlm.nih.gov/15174073/)
- F. Laberge, S. Mühlbrock-Lenter, W. Grunwald, G. Roth, Evolution of the amygdala: New insights from studies in amphibians. *Brain Behav. Evol.* **67**, 177–187 (2006). doi: [10.1159/000091119](https://doi.org/10.1159/000091119); pmid: [16432299](https://pubmed.ncbi.nlm.nih.gov/16432299/)
- N. Moreno, A. González, The common organization of the amygdaloid complex in tetrapods: New concepts based on developmental, hodological and neurochemical data in anuran amphibians. *Prog. Neurobiol.* **78**, 61–90 (2006). doi: [10.1016/j.pneurobio.2005.12.005](https://doi.org/10.1016/j.pneurobio.2005.12.005); pmid: [16457938](https://pubmed.ncbi.nlm.nih.gov/16457938/)
- A. Abellán, E. Desfilis, L. Medina, Combinatorial expression of *Lef1*, *Lhx2*, *Lhx5*, *Lhx9*, *Lmo3*, *Lmo4*, and *Prox1* helps to identify comparable subdivisions in the developing hippocampal formation of mouse and chicken. *Front. Neuroanat.* **8**, 59 (2014). doi: [10.3389/fnana.2014.00059](https://doi.org/10.3389/fnana.2014.00059); pmid: [25071464](https://pubmed.ncbi.nlm.nih.gov/25071464/)
- A. Diodato et al., Molecular signatures of neural connectivity in the olfactory cortex. *Nat. Commun.* **7**, 12238 (2016). doi: [10.1038/ncomms12238](https://doi.org/10.1038/ncomms12238); pmid: [27426965](https://pubmed.ncbi.nlm.nih.gov/27426965/)
- T. J. Neary, "The pallium of anuran amphibians," in *Comparative Structure and Evolution of Cerebral Cortex, Part I*, E. G. Jones, A. Peters, Eds. (Springer, 1990), vol. 8A of *Cerebral Cortex*, pp. 107–138.
- A. Deryckere, J. Woych, E. C. B. Jaeger, M. A. Tosches, Glutamatergic neuron types in the amygdala of the urodele amphibian *Pleurodeles waltl*. *BioRxiv* 496313 [Preprint] (2022). doi: [10.1101/2022.06.15.496313](https://doi.org/10.1101/2022.06.15.496313)
- F. Laberge, G. Roth, Connectivity and cytoarchitecture of the ventral telencephalon in the salamander *Plethodon shermani*. *J. Comp. Neurol.* **482**, 176–200 (2005). doi: [10.1002/cne.20430](https://doi.org/10.1002/cne.20430); pmid: [15611991](https://pubmed.ncbi.nlm.nih.gov/15611991/)
- H. Endepols, K. Roden, W. Walkowiak, Hodological characterization of the septum in anuran amphibians: II. Efferent connections. *J. Comp. Neurol.* **483**, 437–457 (2005). doi: [10.1002/cne.20455](https://doi.org/10.1002/cne.20455); pmid: [15700277](https://pubmed.ncbi.nlm.nih.gov/15700277/)
- A. Joven, A. Simon, Homeostatic and regenerative neurogenesis in salamanders. *Prog. Neurobiol.* **170**, 81–98 (2018). doi: [10.1016/j.pneurobio.2018.04.006](https://doi.org/10.1016/j.pneurobio.2018.04.006); pmid: [29564836](https://pubmed.ncbi.nlm.nih.gov/29564836/)
- G. F. Striedter, R. G. Northcutt, The independent evolution of dorsal pallia in multiple vertebrate lineages. *Brain Behav. Evol.* **96**, 200–211 (2022). doi: [10.1159/000516563](https://doi.org/10.1159/000516563); pmid: [34175847](https://pubmed.ncbi.nlm.nih.gov/34175847/)
- L. Medina, A. Abellán, E. Desfilis, Evolving views on the pallium. *Brain Behav. Evol.* **96**, 181–199 (2022). doi: [10.1159/000519260](https://doi.org/10.1159/000519260); pmid: [34657034](https://pubmed.ncbi.nlm.nih.gov/34657034/)
- F. García-Moreno, Z. Molnár, Variations of telencephalic development that paved the way for neocortical evolution. *Prog. Neurobiol.* **194**, 101865 (2020). doi: [10.1016/j.pneurobio.2020.101865](https://doi.org/10.1016/j.pneurobio.2020.101865); pmid: [32526253](https://pubmed.ncbi.nlm.nih.gov/32526253/)

30. A. Joven *et al.*, Cellular basis of brain maturation and acquisition of complex behaviors in salamanders. *Development* **145**, dev.160051 (2018). doi: [10.1242/dev.160051](https://doi.org/10.1242/dev.160051); pmid: [2921751](https://pubmed.ncbi.nlm.nih.gov/2921751/)
31. T. Stuart *et al.*, Comprehensive integration of single-cell data. *Cell* **177**, 1888–1902.e21 (2019). doi: [10.1016/j.cell.2019.05.031](https://doi.org/10.1016/j.cell.2019.05.031); pmid: [3117818](https://pubmed.ncbi.nlm.nih.gov/3117818/)
32. K. Street *et al.*, Slingshot: Cell lineage and pseudotime inference for single-cell transcriptomics. *BMC Genomics* **19**, 477 (2018). doi: [10.1186/s12864-018-4772-0](https://doi.org/10.1186/s12864-018-4772-0); pmid: [29914354](https://pubmed.ncbi.nlm.nih.gov/29914354/)
33. M. X. Moreau, Y. Saillour, A. W. Cwetsch, A. Pierani, F. Causeret, Single-cell transcriptomics of the early developing mouse cerebral cortex disentangle the spatial and temporal components of neuronal fate acquisition. *Development* **148**, dev197962 (2021). doi: [10.1242/dev.197962](https://doi.org/10.1242/dev.197962); pmid: [34170322](https://pubmed.ncbi.nlm.nih.gov/34170322/)
34. H. Norimoto *et al.*, A claustrum in reptiles and its role in slow-wave sleep. *Nature* **578**, 413–418 (2020). doi: [10.1038/s41586-020-1993-6](https://doi.org/10.1038/s41586-020-1993-6); pmid: [32051589](https://pubmed.ncbi.nlm.nih.gov/32051589/)
35. D. Hain *et al.*, Molecular diversity and evolution of neuron types in the amniote brain. *Science* **377**, eabp8202 (2022).
36. N. Moreno, A. González, Evolution of the amygdaloid complex in vertebrates, with special reference to the anamniote-amniotic transition. *J. Anat.* **211**, 151–163 (2007). doi: [10.1111/j.1469-7580.2007.00780.x](https://doi.org/10.1111/j.1469-7580.2007.00780.x); pmid: [17634058](https://pubmed.ncbi.nlm.nih.gov/17634058/)
37. L. L. Bruce, T. J. Neary, The limbic system of tetrapods: A comparative analysis of cortical and amygdalar populations. *Brain Behav. Evol.* **46**, 224–234 (1995). doi: [10.1159/000113276](https://doi.org/10.1159/000113276); pmid: [8564465](https://pubmed.ncbi.nlm.nih.gov/8564465/)
38. P. R. Manger, D. A. Slutsky, Z. Molnár, Visual subdivisions of the dorsal ventricular ridge of the iguana (*Iguana iguana*) as determined by electrophysiologic mapping. *J. Comp. Neurol.* **453**, 226–246 (2002). doi: [10.1002/cne.10373](https://doi.org/10.1002/cne.10373); pmid: [12378585](https://pubmed.ncbi.nlm.nih.gov/12378585/)
39. D. Arendt *et al.*, The origin and evolution of cell types. *Nat. Rev. Genet.* **17**, 744–757 (2016). doi: [10.1038/nrg.2016.127](https://doi.org/10.1038/nrg.2016.127); pmid: [27818507](https://pubmed.ncbi.nlm.nih.gov/27818507/)
40. E. S. Lein *et al.*, Genome-wide atlas of gene expression in the adult mouse brain. *Nature* **445**, 168–176 (2007). doi: [10.1038/nature05453](https://doi.org/10.1038/nature05453); pmid: [17151600](https://pubmed.ncbi.nlm.nih.gov/17151600/)
41. X. Caubit, M.-C. Tiveron, H. Cremer, L. Fasano, Expression patterns of the three Teashirt-related genes define specific boundaries in the developing and postnatal mouse forebrain. *J. Comp. Neurol.* **486**, 76–88 (2005). doi: [10.1002/cne.20500](https://doi.org/10.1002/cne.20500); pmid: [15834955](https://pubmed.ncbi.nlm.nih.gov/15834955/)
42. A. Zeisel *et al.*, Cell types in the mouse cortex and hippocampus revealed by single-cell RNA-seq. *Science* **347**, 1138–1142 (2015). doi: [10.1126/science.aaa1934](https://doi.org/10.1126/science.aaa1934); pmid: [25700174](https://pubmed.ncbi.nlm.nih.gov/25700174/)
43. Z. Yao *et al.*, A taxonomy of transcriptomic cell types across the isocortex and hippocampal formation. *Cell* **184**, 3222–3241.e26 (2021). doi: [10.1016/j.cell.2021.04.021](https://doi.org/10.1016/j.cell.2021.04.021); pmid: [34004146](https://pubmed.ncbi.nlm.nih.gov/34004146/)
44. G. Fishell, A. Kepcés, Interneuron types as attractors and controllers. *Annu. Rev. Neurosci.* **43**, 1–30 (2020). doi: [10.1146/annurev-neuro-070918-050421](https://doi.org/10.1146/annurev-neuro-070918-050421); pmid: [31299170](https://pubmed.ncbi.nlm.nih.gov/31299170/)
45. N. W. Gouwens *et al.*, Integrated morphoelectric and transcriptomic classification of cortical gabaergic cells. *Cell* **183**, 935–953.e19 (2020). doi: [10.1016/j.cell.2020.09.057](https://doi.org/10.1016/j.cell.2020.09.057); pmid: [33186530](https://pubmed.ncbi.nlm.nih.gov/33186530/)
46. S. Shim, K. Y. Kwan, M. Li, V. Lefebvre, N. Sestan, Cis-regulatory control of corticospinal system development and evolution. *Nature* **486**, 74–79 (2012). doi: [10.1038/nature11094](https://doi.org/10.1038/nature11094); pmid: [22678282](https://pubmed.ncbi.nlm.nih.gov/22678282/)
47. D. Jabaudon, Fate and freedom in developing neocortical circuits. *Nat. Commun.* **8**, 16042 (2017). doi: [10.1038/ncomms16042](https://doi.org/10.1038/ncomms16042); pmid: [28671189](https://pubmed.ncbi.nlm.nih.gov/28671189/)
48. T. Nomura, W. Yamashita, H. Gotoh, K. Ono, Species-specific mechanisms of neuron subtype specification reveal evolutionary plasticity of amniote brain development. *Cell Rep.* **22**, 3142–3151 (2018). doi: [10.1016/j.celrep.2018.02.086](https://doi.org/10.1016/j.celrep.2018.02.086); pmid: [29562171](https://pubmed.ncbi.nlm.nih.gov/29562171/)
49. N. Moreno, R. Morona, J. M. López, A. González, in *Evolution of Nervous Systems* (Elsevier, 2017), pp. 409–426.
50. A. Joven, R. Morona, N. Moreno, A. González, Regional distribution of calretinin and calbindin-D28k expression in the brain of the urodele amphibian *Pleurodeles waltli* during embryonic and larval development. *Brain Struct. Funct.* **218**, 969–1003 (2013). doi: [10.1007/s00429-012-0442-1](https://doi.org/10.1007/s00429-012-0442-1); pmid: [22843286](https://pubmed.ncbi.nlm.nih.gov/22843286/)
51. E. Lanuza, M. Belekhova, A. Martínez-Marcos, C. Font, F. Martínez-García, Identification of the reptilian basolateral amygdala: An anatomical investigation of the afferents to the posterior dorsal ventricular ridge of the lizard *Podarcis hispanica*. *Eur. J. Neurosci.* **10**, 3517–3534 (1998). doi: [10.1046/j.1460-9568.1998.00363.x](https://doi.org/10.1046/j.1460-9568.1998.00363.x); pmid: [9824465](https://pubmed.ncbi.nlm.nih.gov/9824465/)
52. P. Cordery, Z. Molnár, Embryonic development of connections in turtle pallium. *J. Comp. Neurol.* **413**, 26–54 (1999). doi: [10.1002/\(SICI\)1096-9861\(1999101\)413:1<26::AID-CNCE2>3.0.CO;2-N](https://doi.org/10.1002/(SICI)1096-9861(1999101)413:1<26::AID-CNCE2>3.0.CO;2-N); pmid: [10464368](https://pubmed.ncbi.nlm.nih.gov/10464368/)
53. T. J. Voneida, C. M. Sligar, Efferent projections of the dorsal ventricular ridge and the striatum in the Tegu lizard, *Tupinambis nigropunctatus*. *J. Comp. Neurol.* **186**, 43–64 (1979). doi: [10.1002/cne.901860104](https://doi.org/10.1002/cne.901860104); pmid: [457930](https://pubmed.ncbi.nlm.nih.gov/457930/)
54. M. P. Witter, T. P. Doan, B. Jacobsen, E. S. Nilssen, S. Ohara, Architecture of the entorhinal cortex: A review of entorhinal anatomy in rodents with some comparative notes. *Front. Syst. Neurosci.* **11**, 46 (2017). doi: [10.3389/fnsys.2017.00046](https://doi.org/10.3389/fnsys.2017.00046); pmid: [28701931](https://pubmed.ncbi.nlm.nih.gov/28701931/)
55. T. P. O’Leary *et al.*, Extensive and spatially variable within-cell-type heterogeneity across the basolateral amygdala. *eLife* **9**, e59003 (2020). doi: [10.7554/eLife.59003](https://doi.org/10.7554/eLife.59003); pmid: [32869744](https://pubmed.ncbi.nlm.nih.gov/32869744/)
56. T. J. Johnston, The development of the dorsal ventricular ridge in turtles. *J. Comp. Neurol.* **26**, 481–505 (1916). doi: [10.1002/cne.900260504](https://doi.org/10.1002/cne.900260504)
57. F. C. Leitner *et al.*, Spatially segregated feedforward and feedback neurons support differential odor processing in the lateral entorhinal cortex. *Nat. Neurosci.* **19**, 935–944 (2016). doi: [10.1038/nn.4303](https://doi.org/10.1038/nn.4303); pmid: [27182817](https://pubmed.ncbi.nlm.nih.gov/27182817/)
58. M. A. Tosches, From cell types to an integrated understanding of brain evolution: The case of the cerebral cortex. *Annu. Rev. Cell Dev. Biol.* **37**, 495–517 (2021). doi: [10.1146/annurev-cellbio-120319-112654](https://doi.org/10.1146/annurev-cellbio-120319-112654); pmid: [34416113](https://pubmed.ncbi.nlm.nih.gov/34416113/)
59. F. Luzzati, A hypothesis for the evolution of the upper layers of the neocortex through co-option of the olfactory cortex developmental program. *Front. Neurosci.* **9**, 162 (2015). doi: [10.3389/fnins.2015.00162](https://doi.org/10.3389/fnins.2015.00162); pmid: [26029038](https://pubmed.ncbi.nlm.nih.gov/26029038/)
60. S. Bloch *et al.*, Non-thalamic origin of zebrafish sensory nuclei implies convergent evolution of visual pathways in amniotes and teleosts. *eLife* **9**, e54945 (2020). doi: [10.7554/eLife.54945](https://doi.org/10.7554/eLife.54945); pmid: [32896272](https://pubmed.ncbi.nlm.nih.gov/32896272/)
61. S. M. Suryanarayana, B. Robertson, P. Wallén, S. Grillner, The lamprey pallium provides a blueprint of the mammalian layered cortex. *Curr. Biol.* **27**, 3264–3277.e5 (2017). doi: [10.1016/j.cub.2017.09.034](https://doi.org/10.1016/j.cub.2017.09.034); pmid: [29056451](https://pubmed.ncbi.nlm.nih.gov/29056451/)
62. J. Fournier, C. M. Müller, I. Schneider, G. Laurent, Spatial information in a non-retinotopic visual cortex. *Neuron* **97**, 164–180.e7 (2018). doi: [10.1016/j.neuron.2017.11.017](https://doi.org/10.1016/j.neuron.2017.11.017); pmid: [29249282](https://pubmed.ncbi.nlm.nih.gov/29249282/)
63. Code for: J. Woyach, A. Ortega Gurrola, A. Deryckere, E. C. B. Jaeger, E. Gumnit, G. Merello, J. Gu, A. Joven Araus, N. D. Leigh, M. Yun, A. Simon, M. A. Tosches, Cell-type profiling in salamanders identifies innovations in vertebrate forebrain evolution, Zenodo (2022); doi: [10.5281/zenodo.6780577](https://doi.org/10.5281/zenodo.6780577)

ACKNOWLEDGMENTS

We thank J. Barber, S. Cook, and the Columbia University Institute of Comparative Medicine for animal care; B. Jekely for help with cloning; E. Subramanian for contributing to the IsoSeq reference; A. Matheson for the diagram in fig. S19, B and C; and A. Matheson, L. Xu, G. Laurent, O. Hobert, and R. Satija for critical feedback on the manuscript. Light-sheet imaging was performed with support from L. Hammond and the Zuckerman Institute’s Cellular Imaging platform (NIH grant 1S10OD023587-01). Computing resources were provided by Columbia University’s Shared Research Computing Facility (NIH grant 1G2ORRO30389-01 and NYSTAR contract C090171). The National Genomics Infrastructure (NGI)/Uppsala Genome Center and UPPMAX provided assistance in massive parallel sequencing and computational infrastructure. Work performed at the NGI/Uppsala Genome Center was funded by the Swedish Council for Research Infrastructure and the Science for Life Laboratory (Sweden). Storage and handling of IsoSeq data were enabled by resources provided by the Swedish National Infrastructure for Computing (SNIC) at UPPMAX, which is partially funded by the Swedish Research Council through grant 2018-05973. **Funding:** This work was supported by the McKnight Foundation (M.A.T.), the NIH (grant NHGRI RMIHG011014 to M.A.T.), the National Science Foundation (Graduate Research Fellowship DGE 2036197 to E.C.B.J.), the Knut and Alice Wallenberg Foundation (A.S.), and the European Research Council (A.S.). **Author contributions:** J.W., A.O.G., A.D., and E.G. produced the scRNA-seq data. E.G., A.O.G., M.A.T., and J.G. analyzed the scRNA-seq data. A.J.A., N.D.L., A.S., and M.Y. assembled the IsoSeq transcriptome. J.W., A.D., E.C.B.J., and G.M. analyzed the anatomy and histology. J.W., E.C.B.J., and A.D. produced and analyzed axonal tracing data. M.A.T., A.D., E.C.B.J., A.O.G., J.W., and E.G. wrote the manuscript. A.J.A., A.S., N.D.L., and M.Y. edited the manuscript. M.A.T. provided project management and supervised the study.

Competing interests: The authors declare no competing interests.

Data and materials availability: The scRNA-seq data used in this study have been deposited in the Gene Expression Omnibus (GEO) with accession numbers GSE197701, GSE197722, GSE197796, GSE197807, GSE198363, GSE198364, GSE198366, GSE198367, GSE198365, and GSE206163. The IsoSeq data are accessible on NIH Sequence Read Archive (SRA) with accession number SRX1625271. All other data are included in the main paper or the supplementary materials. Code used for the analysis of scRNA-seq data is available at Zenodo (63). A website to access the data and search genes of interest is available at https://toscheslab.shinyapps.io/salamander_teiencephalon/. **License information:** Copyright © 2022 the authors, some rights reserved; exclusive licensee American Association for the Advancement of Science. No claim to original US government works. <https://www.science.org/about/science-licenses-journal-article-reuse>

SUPPLEMENTARY MATERIALS

science.org/doi/10.1126/science.abp9186

Materials and Methods

Supplementary Text

Figs. S1 to S19

References (64–94)

Movies S1 to S3

Data S1

MDAR Reproducibility Checklist

View/request a protocol for this paper from Bio-protocol.

Submitted 7 March 2022; accepted 12 July 2022

10.1126/science.abp9186